STEM CELLS®

STEM CELL TECHNOLOGY: EPIGENETICS, GENOMICS, PROTEOMICS AND METABONOMICS

Surfaceome Profiling Reveals Regulators of Neural Stem Cell Function

Brian DeVeale[1*], Damaris Bausch-Fluck[2], Raewyn Seaberg[3], Susan Runciman[1], Vahe Akbarian[4], Phillip Karpowicz[5], Charles Yoon[4], Hannah Song[4], Rachel Leeder[3], Peter W. Zandstra[4], Bernd Wollscheid[2] and Derek van der Kooy[1*]

[1]Department of Molecular Genetics, University of Toronto, Toronto, Ontario, Canada, M5S 1A8, [2]ETH Zurich, Institute of Molecular Systems Biology, NCCR Neuro Center for Proteomics, Zurich CH–8093, Switzerland; [3]Institute of Medical Science, University of Toronto, Toronto, Ontario, Canada, M5S 1A8; [4]Institute of Biomaterials and Biomedical Engineering, University of Toronto, Toronto, ON, Canada; [5]Department of Genetics, Harvard Medical School, Boston, Massachusetts, USA

Key Words. Neural Stem Cells • Membrane Glycoproteins • Embryonic Development • Developmental gene expression regulation

ABSTRACT

The composition of cell-surface proteins changes during lineage specification, altering cellular responses to their milieu. The changes that characterize maturation of early neural stem cells (NSCs) remain poorly understood. Here we use mass-spectrometry (MS) based Cell Surface Capture (CSC) technology to profile the cell surface of early NSCs and demonstrate functional requirements for several enriched molecules. Primitive NSCs arise from embryonic stem (ES) cells upon removal of TGF-β signaling, whilst definitive NSCs arise from primitive NSCs upon Lif removal and FGF addition. *In vivo* aggregation assays revealed that N-cadherin upregulation is sufficient for the initial exclusion of definitive NSCs from pluripotent ectoderm, while c-kit signaling limits progeny of primitive NSCs. Further, we implicate EphA4 in primitive NSC survival signaling and Erbb2 as being required for NSC proliferation. This work elucidates several key mediators of NSC function whose relevance is confirmed on forebrain-derived populations and identifies a host of other candidates that may regulate NSCs.

INTRODUCTION

During mammalian development lineages diverge from pluripotent epithelium and acquire cell-autonomous properties including distinct adhesive profiles that facilitate morphogenetic movements and cell-sorting as well as distinct arrays of receptors which restrict the range and output of morphogen responsiveness. Cell surface protein composition at the earliest stages of NSC development is poorly understood, and improved characterization would help elucidate the regulators of critical NSC properties. A comprehensive surfaceome profile of NSCs would provide a starting point to *in vivo* identification, purification, and manipulation of

Author contributions: B.D.: conception, experimentation, manuscript writing; D.B.F.: experimentation, manuscript writing; R.S.: experimentation; S.R.: experimentation; V.A.: experimentation; P.K.: experimentation; C.Y.: experimentation; H.S.: experimentation; R.L.: experimentation; P.W.Z.: conception; B.W.: conception, manuscript authoring, funding; D.v.d.K.: conception, manuscript authoring, funding
Contact Information: Brian DeVeale, Donnelly CCBR, University of Toronto, 160 College Street, rm 1110, Toronto ON, M5S 3E1, *brian.deveale@utoronto.ca, derek.van.der.kooy@utoronto.ca, 416.978.1960 (lab); 416.978.2666 (fax); Funding: Canadian Institute for Health Research (CIHR) 'Cell Lineage and Brain Development' awarded to (D.v.d.K.), and 'Neural Plasticity and Repair' from the National Center of Competence in Research (NCCR) to (B.W.).; Received January 23, 2013; accepted for publication July 24, 2013; 1066-5099/2013/$30.00/0 doi: 10.1002/stem.1550

NSCs. At present, the means of selectively manipulating the function of rare NSCs are limited, in part because so few markers are known.

Neural tissue is induced and segregated from ectoderm by release of bone morphogenetic protein (BMP) antagonists such as Noggin and Chordin from anterior visceral endoderm at E7.5 of murine development [1]; BMP antagonism effectively relieves repression of neural fate, as factors downstream of BMPs including SMADs and inhibitors of differentiation (ID) inhibit the neural program [2, 3]. These events can be modeled using pluripotent ES cells that self-renew when cultured with BMP4 and Leukemia inhibitory factor (Lif) [4], but undergo neural induction when placed at low density in serum free media with Lif but without exogenous BMPs [3]. Greater than 90% of ES cells which survive in pNSC culture conditions translate sufficiently abundant Sox1, a specific neural marker, after 20hrs that it is detectable by immunohistochemistry [5], consistent with Lif signaling through Stat3 mediating a block of non-neural differentiation via Nanog [2, 4, 6, 7].

Lif-dependent NSCs arise coincident with neural specification at E7.5 then decrease in abundance at E8.5, coincident with an increase in the prevalence of FGF-dependent NSCs that persist through adulthood [8]. When ES cells are transferred from self-renewal conditions to serum-free media with Lif, a subset referred to as primitive NSCs (pNSCs) proliferate extensively as clones [3]. pNSCs produce definitive NSC (dNSCs) that are not Lif-dependent, but require exogenous FGF comparable to embryo-derived NSCs [3]. FGF is required for proliferation of neural populations [5, 9] and downstream signaling via ERK –at least transiently- contributes to neural maturation [10]. We reasoned that an unbiased profile of the cell-surface constituents of each cell in the early NSC lineage and functional interrogation would help elucidate the molecules that dictate their respective identities.

Here we profile the cell surface of ES cells, pNSCs and dNSCs in this clonally derived sequential neural lineage using CSC technology to identify glycosylated plasma membrane proteins with MS [11]. We also demonstrate the utility of this data in making predictions about protein function in NSCs. Specifically, we demonstrate that Neural-cadherin (N-Cad) is sufficient for exclusion of dNSC from the pluripotent inner cell mass (ICM), that c-kit signaling limits NSC-derived progeny, perhaps by promoting pNSC quiescence or limiting specification of alternative fates, that signaling through EphA4 is required for viability of pNSC populations and that Erbb2 signaling is required for the proliferation of NSCs. Moreover, we show the relevance of these findings to NSCs derived from adult mice.

RESULTS

Cell surface profiling reveals distinct NSC signatures

Discrepancies exist between the abundance of protein and corresponding mRNAs [12]. These data suggest that meaningful regulation of protein profiles occurs at the level of translation and supports the merit of directly assessing proteins for both identification and quantification.

During development, lineage maturation and terminal differentiation are governed by a variety of factors including adhesion molecules that dictate cell-sorting and receptors that dictate morphogen responsiveness. Proteins at the cell surface are of particular interest in understanding these processes since they mediate cell-cell communication, signal transduction, migration and adhesion. To elucidate plasma membrane proteins involved in maturation of the neural lineage, we compared the cell surface protein profile of ES, pNSCs and dNSCs using CSC [11, 13]. CSC offers a major advantage over antibody profiling approaches to cell-surface protein characterization in that CSC enables protein identification and relative quantification of the broad spectrum of plasma membrane

glycoproteins in parallel. As such, the technique offers insight into the complement of environmental stimuli to which cells may be responsive independent of the antibodies available for detection. Moreover, CSC distinguishes itself from comparable MS-based techniques in that labeling is performed on viable cells. In brief, the glycans of plasma membrane proteins were labeled, purified with streptavidin, then enzymatically released and identified by reverse-phase liquid chromatography coupled to tandem MS (LC MS/MS).

Using CSC and LC MS/MS, 813, 1134 and 880 peptides were detected in the three respective cellular subsets (ES, pNSCs, dNSCs). After collapsing peptides that mapped to the same protein, a total of 378, 563 and 456 proteins were identified using Occam's razor approach of ProteinProphet with a false-discovery rate (FDR) of <0.01 (Fig 1A). In each cell type over 200 membrane glycoproteins were identified, many of these are shared between the three cell types (Fig 1B).

In order to quantify the differential expression of the cell surface proteins, we analyzed them by label-free quantification [14] with Progenesis software. We focused on those proteins that were identified via at least one peptide containing the N-glycosylation motif: asparagine, any amino acid, serine or threonine (NXS/T) and a deamidation on this asparagine. Such motifs are a distinguishing feature of cell surface proteins compared to cytoplasmic proteins in that most cell surface proteins are N-glycosylated [15, 16]. Since we specifically target, enrich and modify such glycopeptides during the CSC workflow, their specific and repetitive identification is strong evidence of the cell surface location of the respective protein at the time of labeling.

Overall, 228 proteins were quantified which differed significantly ($p<0.05$) in relative abundance between at least two of the three cell types. Use of precursors from within the same sequential lineage as background during comparisons with NSCs should enrich for differences that define the biology of each distinct NSC in the lineage. Proteins that are significantly ($p<0.05$) different and a minimum of 5 times more abundant based on the MS signal in one cell type in the lineage than in either of the other two are depicted in Figure 1C (150 proteins). Proteins are connected by an edge to the cell type in which they are 5 times higher [17]. More detailed summaries of the top 20 proteins by fold enrichment in NSCs can be found in supplementary (S) Table S1-3, and a complete list of peptides with their corresponding normalized abundance in each cell type can be found in Dataset S1.

Cell surface protein profiling yielded enrichment of proteins whose relevance in the NSC lineage is established. Prominin, a cell surface marker commonly used for neural precursor enrichment [18] exhibited 50 times the MS signal intensity in pNSC than ES cells and 95 times the signal intensity in dNSC than ES cells. While the ratio of signal intensity between cell types is not an exact readout of the fold difference in copy number for a particular protein between cell types, it is an accurate predictor of up- or down-regulation and can be used to estimate the magnitude of these differences. Several components of the hedgehog signaling pathway (Hh), known to be important in NSC function, were upregulated in NSCs; these included hedgehog-interacting protein (HhIP) which is 813 times higher in dNSC than ES cells ($p<0.05$), as well as Smoothened (Smo) which is 18 times higher in dNSCs than ES cells and Patched 1 which is 12 times higher in dNSCs than ES cells. Similarly, EphA4, which is an established mediator of viability in the adult subependymal [19, 20] was 31 times higher in pNSC than ES cells ($p<0.05$). As expected, lineage markers of NSC-progeny are also upregulated in the surfaceome profile. For example, CD24, a marker of NSC-derived neuroblasts that is expressed specifically in the adult subependymal zone [21, 22], was 25 times higher ($p<0.05$) in dNSCs compared to ES populations based on the MS signals. While the

numerical accuracy of differences in protein abundance between cell types would be improved by additional repetitions and absolute quantitative Selective Reaction Monitoring assays using internal standards [23] they are useful estimates and suggest that the profiling data are likely to contain other molecules relevant to the biology of NSCs.

Increased N-Cadherin is sufficient for exclusion of dNSCs from ectoderm

The greatest relative difference in abundance detected between dNSCs and their precursor pNSCs through CSC profiling was in N-cad, a calcium dependent adhesion molecule where we detected an MS signal 5850 times higher in dNSCs (Fig 3A and Table S3). Adhesive differences between cell types are essential during development to organize tissues and signaling niches. To assess whether the differences in adhesion molecules detected by MS are functionally relevant and constitute candidate mediators of NSC sorting from unspecified ectoderm, we performed morula aggregation assays. The intent was to test whether increased N-cad was sufficient to exclude NSCs from the pluripotent ICM. Knowing that ES cells will colonize the ICM when aggregated with morula, we started by asking whether the two neural populations in the lineage were equally proficient in doing so. pNSC colonies incorporated within the ICM 88% (n=1302/1486) of the time, comparable to the 89% rate of ES cells (n=146/164) (Fig 2B). Conversely, dNSC colonies rarely colonize the ICM (n=33/814) (Fig 2B).

To assess whether the difference in adhesive compatibility between pNSC and dNSC was due to the loss of Lif signaling or addition of FGF + B27, we assessed the adhesive properties of pNSCs passaged into Lif, FGF and B27. Under these culture conditions, NSCs colonized the ICM in 51% (n=391/769) of cases indicating that loss of Lif-based signaling is important, but not solely responsible for the altered adhesive profile of dNSCs (Fig 2B).

E-cadherin (E-cad) is primarily responsible for adhesion of preimplantation embryos [24], suggesting that Lif-dependent colonization of the ICM by dNSCs might be due to maintenance of E-cad by Lif. Because the NXS/T motif used to select membrane proteins is absent in a small subset of surface bound proteins, including E-cad, we estimated its relative abundance by quantitative PCR (Fig 2C). E-cad transcript abundance declines in ES-derived dNSCs as it does during lineage maturation of NSCs *in vivo* [25]. However addition of Lif to dNSC cultures did not maintain the E-cad levels of ES and pNSCs ($p<0.05$), indicating E-cad is not responsible for the Lif-dependent rescue of ICM colonization by dNSCs.

To test the prediction that adhesion molecules showing elevated expression in dNSCs relative to ES and pNSCs mediated the exclusion of dNSCs from ectoderm, we blocked N-cad, which showed the greatest difference in abundance between dNSCs and their precursor population, pNSCs. We previously observed upregulation of N-cad in embryonic and adult NSC populations relative to ES cells suggesting that this feature of the *in vitro* model recapitulates development [25]. Culturing dNSCs in an N-cad function-blocking antibody partially 'rescued' their ability to colonize the ICM (Fig 3B). Confirmation that rescued cells made bona fide contributions to the ICM was achieved by confocal microscopy in all 8 samples that were optically sectioned. A sample confocal stack of rescued dNSC aggregation is shown in Fig 3D. While the minimal culture conditions employed in these cell and embryo-culture experiments are not physiological, they are ideal for teasing apart biology that may be buffered by redundancies *in vivo*. Despite being heterochronic, we note that these experiments collectively suggest that the N-cad upregulation contributes to exclusion of dNSCs from the pluripotent ectoderm.

Cell surface protein profiling identifies molecules required specifically for NSC function

We reasoned that molecules enriched in NSCs relative to the ES cells from which they were derived might mediate functions specifically in NSCs. For further analysis, we chose candidates that are 5 times enriched in either pNSCs or dNSCs relative to ES cells ($p<0.05$) and had an available selective inhibitor. To assay whether enrichment within the neural populations predicted functionally relevant molecules, we compared the colony-forming ability of ES cells to each of the pNSC and dNSC populations in the presence of inhibitors targeting candidates of interest. Inhibition that selectively affected NSCs, but not ES cells, would suggest the candidate mediated proliferation, survival, quiescence, or cell fate specification of NSCs. These possibilities can be distinguished by additional experimentation. Colony formation in each inhibitor was normalized to the appropriate vehicle control at a concentration of inhibitor previously established to be selective for the target (see Materials and Methods for detail) [26-30].

Of the proteins enriched on the cell surface of NSCs compared to ES cells, we chose inhibitors directed against N-cad, Hh, EphA4, Erbb2 and c-kit. Aside from the N-cad function blocking antibody, each of these had significant effects on at least one of the ES-derived NSC populations without affecting ES cells ($F_{3,15} = 8.27$, $p<0.05$). Inhibition of Hh, a pathway whose relevance to NSCs *in vivo* is established [31], blocked formation of both pNSCs and dNSCs without affecting ES cells ($p<0.05$)(Fig 4A). This indicates that aspects of the *in vivo* lineage are being recapitulated effectively. Similarly, EphA4 has been implicated in viability of subependymal NSCs, and inhibition blocked dNSC colony formation without affecting ES colony growth ($p<0.05$)(Fig 4A). Conversely, the same N-cad function-blocking antibody that disrupted adhesion of NSCs (Fig 3D) did not impact functions assayable in this experiment: N-cad inhibition had no effect on colony formation of either pNSCs or dNSCs ($p>0.05$). An earlier role for EphA4 had not been explored previously, and we found that pNSCs exhibited a comparable response to dNSCs in requiring EphA4 for colony formation ($p<0.05$)(Fig 4A). Erbb2 has not been implicated in NSC biology previously, and blocked formation of pNSC colonies ($p<0.05$)(Fig 4A). This assay also revealed a novel function of c-kit signaling in NSC biology: its inhibition selectively increased colony formation of pNSCs ($p<0.05$)(Fig 4A). The novel effects of the inhibitors on colony formation by pNSCs and dNSCs were specific to NSCs and unrelated serum-based ES culture media as repetition of the experiment culturing ES colonies in serum free conditions [32] and inhibiting Erbb2, EphA4 or c-Kit yielded the same NSC-specific effects (Fig S1).

We then asked whether the inhibitors were blocking signaling involved in viability or proliferation. Hh mediates ventricular-derived dNSC proliferation [33]. We found that Hh inhibition reduced pNSC viability and prevented division, suggesting that Hh mediates both NSC viability and proliferation (Fig 4B). EphA4 inhibition led to increased cell death of both pNSCs and dNSCs (Fig 4B), suggesting that signaling through EphA4 is required for NSC viability. Conversely, Erbb2 inhibition did not have an effect on pNSC viability but limited division, indicating its signaling requirement for proliferation (Fig 4B). Finally, c-kit inhibition did not have an appreciable affect on viability or the colony size of pNSCs (Fig 4B and C), suggesting that c-kit signaling regulates another property, perhaps pNSC specification or quiescence. Indeed, profiling by flow cytometry suggests that c-kit is present during the transition from ES cells to pNSCs before decreasing in abundance during NSC maturation (Fig S2).

Next, we asked whether the molecules that affected the ES-derived NSCs were relevant to murine forebrain-derived populations. Using the same doses that affected ES-derived NSCs but did not impair ES colony formation, 3 of the 4 inhibitors blocked colony formation from

forebrain derived NSCs, supporting the relevance of predictions made with the *in vitro* model to the *in vivo* case (Fig 4A). Indeed, inhibition of c-kit by Gleevec –the lone inhibitor that did not produce an effect on aNSCs— enhanced colony formation of pNSCs from postnatal day 7 pups (unpublished data), supporting the relevance of this model, and suggesting that the effect is mediated through quiesence. While EphA4 and Hh are established mediators of NSCs *in vivo*, this work implicates c-kit in the biology of pNSCs and Erbb2 in the biology of adult mouse-derived NSCs.

To ensure that the proposed candidates were responsible for the effects on NSCs, we repeated the colony forming assays, targeting the candidates with siRNAs. Depletion of the transcripts of interest was confirmed by QPCR (Fig 5A,B). The effects on colony formation observed using inhibitors were confirmed with siRNA (Fig 5C), supporting implication of the intended targets in NSC biology. An overall summary of these observations is provided in Fig 6.

DISCUSSION

Direct glycoprotein profiling of NSCs bypassed the incongruency inherent in making inferences about protein abundance from transcriptional profiling [12], and revealed novel regulators in this lineage. The veracity of this model and profiling approach is demonstrated by markers presently used to enrich neural stem/progenitors from mice (prominin and CD24) being enriched in dNSCs relative to ES cells. This approach contributed to the identification of several molecules for which we have experimentally demonstrated biological roles in the earliest NSC populations, suggesting that the remainder of the profile is also likely to be rich in mediators of NSC behavior.

Our data support a model where N-cad is upregulated upon loss of Lif/Stat3 signal transduction, altering the adhesive profile of dNSCs such that they are excluded from adjacent ectoderm. N-cad is expressed in several tissues within the developing embryo, including the neural plate from ~E7.5, consistent with the possibility that N-cad mediates segregation of early neural cell types from other lineages. The observation that pNSCs, cultured in SFM + Lif, maintain a comparable ability to colonize the ICM as ES cells indicates that loss of BMP plays a minor role, if any, in the upregulation of N-cad. Furthermore, while dNSCs cultured in FGF-containing media almost entirely lose the ability to colonize the ICM, addition of Lif results in a partial rescue of ICM compatibility. These data, combined with the observation that addition of Lif to dNSC culture does not maintain E-cad levels equivalent to that of ES cells, suggests that Lif signal transduction is critical to maintaining the low N-cad levels required for ectoderm integration. That the Lif based rescue of dNSC compatibility is only partial suggests that FGF and/or other signaling may also be involved in the adhesive profile transition. Indeed, the transition from ES to Epiblast stem cells (EpiSCs) is characterized by Lif removal, FGF addition and a corresponding decrease in ICM colonization [34, 35], while the combination of both Lif and BMP appears to induce ICM competence or reversion from EpiSCs [36]. EpiSC cultures are supplemented with Activin A to prevent neuralization and maintain pluripotency, distinguishing them from the default entry into the neural lineage exhibited by the pNSCs and dNSCs in this study [34, 35]. Our data suggest that Lif-mediated activation of JAK/STAT and/or MAPK signaling cascades is responsible for maintaining low N-cad expression that is compatible with ICM colonization.

Selective inhibition implicated several other candidates from the MS profiling in aspects of NSC function. In agreement with the independent conclusion that Ephrin B3 signaling through Epha4 promotes cell viability in the adult subependymal [19, 20], we found that EphA4 is required in adult-derived NSCs and ES-derived dNSCs for viability. In addition to these recapitulations, we report for the first time

that EphA4 is required for viability of the early pNSC population. Conversely, c-kit inhibition increases the frequency of colony-formation by pNSCs but neither ES-derived dNSCs nor forebrain-derived dNSCs. c-kit might promote specification of alternative cell fates, asymmetric divisions, or quiescence of pNSCs, perhaps as regulator of the population size. Erbb2 inhibition blocks colony formation of ES-derived NSCs as well as adult dNSCs. Erbb2 ligand Nrg-1 is required for proliferation of neural precursors [37], although the specific requirement for Erbb2, as opposed to another Nrg-1 receptor Erbb4, was not shown previously.

This study demonstrates the value of using CSC technology on viable cells and sequential, clonal precursor populations as a background to ascertain biologically relevant changes in cell-surface protein profiles during lineage maturation. We demonstrated functional roles for four proteins showing increased abundance during the maturation of ES cells into NSCs. These represent a small fraction of the 112 peptides in this dataset that showed significant ($p<0.05$) enrichment (5 times). Such confirmations, along with detection of high enrichment in proteins known to specifically mediate NSC functions such as EphA4 (31 times dNSC/ES) and Hh components (HhIP, Smo and Ptch1 were all >10 times dNSC/ES), suggest that the remainder of the dataset also will be rich in proteins relevant to NSC biology, and the earliest events in neural induction. Fruitful approaches to systematically exploring the biology of each cell type might include screening the list of candidates from this profile using antibody-based selection to test for enrichment of populations of interest from within the brain germinal zone populations or the use of siRNAs to determine molecules required for viability and proliferation. As such, this dataset is a step towards a higher resolution understanding of NSC biology.

EXPERIMENTAL PROCEDURES

Cell Culture

R1 ES cells (a gift from A. Nagy) were used for experiments unless otherwise specified. For maintenance, ES cells were grown on mitotically inactive embryonic fibroblast layers in DMEM plus 15% fetal calf serum (FCS)(Hyclone) culture medium containing LIF (1000 U/ml; Millipore). pNSCs and dNSCs were generated as described in [3]. For CSC profiling, R1 ES cells were passaged three times to expand from a starting population of ~$1x10^6$ cells to ~$5x10^7$ ES cells before seeding pNSC cultures. Each population of cells analyzed by CSC ranged from $1x10^8$ – $6x10^8$ cells. YC5/eYFP ES cells (a gift from A. Nagy) were used to generate pNSC and dNSCs for aggregation experiments [38].

For the colony formation assays assessing the effect of small molecule inhibitors and siRNA, ES cells were plated in DMEM + 15% fetal calf serum (Hyclone) and Lif (1000U/ml; Millipore) on gelatin coated plates [39]. pNSCs and dNSCs were plated in serum free media supplemented with Lif (1000U/ml; Millipore) or FGF2 (10ng/ml; Sigma) + Heparin (2µg/ml; Sigma) + B27 (1:50; Invitrogen) respectively [3, 5]. Colonies ≥50µm in diameter were counted in the quantification. Exclusively for the comparison of ES cells cultured in serum free media (Fig S1), ES cells were grown on gelatin in '2i' media 3uM chir99021 (Reagents Direct) and 1uM PD0325901 (Reagents Direct)) [32].

Inhibitor Assays Inhibitors were added to the cultures during plating. EphA4 blocking peptide (Alta Biosciences), Erbb2 inhibitor II (Calbiochem), Gleevec (Toronto Research Chemicals Inc.), N-cad function blocking antibody (Sigma) or Cyclopamine (Toronto Research Chemicals Inc.) that were dissolved in PBS, DMSO, DMSO, PBS and EtOH respectively. Control inhibitors were applied at the high end of the established efficacy range: Cyclopamine efficacy increases up to 10µM in some assays [27, 40], so it was applied at 5µM; efficacy of the N-cad antibody was titrated

previously [30], and half the maximal dose (1ug/ml) applied. Inhibitors of candidate molecules were applied at concentrations ensuring efficacy and maintaining specificity to the extent possible. 50μM exceeds the concentration providing maximal inhibition of ephrin binding by the EphA4 function blocking peptide in one assay (~10μM), but was used to ensure efficacy as it retains specificity for EphA4 over other Eph-family receptors [41]. The reported IC_{50} of Gleevec varies from 0.2μM [42, 43] to 9.5μM [44] dependent on the cell type and assay. Gleevec is known to inhibit multiple kinases at concentrations where it inhibits c-kit function [43], but escalating efficacy with respect to c-kit inhibition has been observed above 2μM [26], so we chose 4μM to ensure efficacy. Depending on the cell type and assay, the reported IC_{50} of the Erbb2 inhibitor II (Calbiochem) ranges from 6μM to 30.9μM (Calbiochem). At concentrations below 100μM, inhibition is specific for Erbb2, and not other Erb family members (Calbiochem). Viability was assessed using trypan blue exclusion after 24hrs. Proliferation deficits were inferred in situations where inhibitors did not cause significant effects on viability but did prevent sphere formation. Viability and proliferation of ES cells was assessed on both gelatin (Millipore) and mitotically inactivated feeders.

siRNA Assays. All siRNAs were obtained from Dharmacon and used according to the manufacturer's instructions. Each treatment group received siRNA for 2 days before the beginning of the colony forming assay. For example, application of siRNA to pNSCs consisted of treating ES cells for 2 days with a particular siRNA and then applying the same siRNA to pNSC for the duration of their 7 day culture period. All siRNAs were applied at a final concentration of 50nM, along with DharmaFECT1 (1:500). The following were used: cKit ON-TARGETplus siRNA J-042174-05-0010; Erbb2 ON-TARGETplus siRNA J-064147-05-0010; EphA4 ON-TARGETplus siRNA J-055030-05-0010; Scramble ON-TARGETplus Non-targeting siRNA #1

Cell surface capturing

CSC was performed as described previously [11]. In brief, colonies were dissociated by manual trituration after incubation in 1mM EDTA and 10% FBS (Hyclone) for 15min at 37°C. Extracellularly exposed aldehydes were then oxidized with 1.6mM sodium meta-periodate (NaIO4) (Piercenet) and reacted for 1 hour with 5mM biocytin hydrazide (Biotium.com). The cells were then washed and lysed by dounce homogenization in a hypotonic lysis buffer and the nuclei were pelleted by centrifugation. The supernatant containing the membranes and the cytoplasm was mixed with membrane prep buffer (280 mM sucrose, 50 mM MES pH 6, 450 mM NaCl, 10 mM MgCl2) and subjected to ultra centrifugation. The microsomal pellet was collected after 1 hour centrifugation at 35 000 rpm and solubilized by addition of 0.1% RapiGest (Waters) and sonification. After overnight trypsin digestion, the biontinylated peptides were coupled to streptavidin beads (Piercenet), thoroughly washed and released by PNGaseF (NEB), which cleaves N-glycosylated peptides at their backbone. Peptides were then clean-up over C18-tips (The NestGroup) and subjected to reverse-phase liquid chromatography coupled to tandem MS.

Mass spectrometry

Each peptide sample was analyzed on an Eksigent Nano LC system (Eksigent Technologies) connected to a hybrid linear ion trap LTQ Orbitrap (Thermo Scientific) mass spectrometer, which was equipped with a nanoelectrospray ion source (Thermo Scientific). Peptide separation was carried out on a RP-HPLC column (75 μm x 10 cm) packed in-house with C18 resin (Magic C18 AQ 3 μm, Michrom BioResources) using a linear gradient from 90 % solvent A (water, 0.2 % formic acid, 1 % acetonitrile) and 10 % solvent B (water, 0.2 % formic acid, 80 % acetonitrile) to 65 % solvent A and 35 % solvent B over 60 min at a flow rate of 0.2 μl/ min. The data acquisition mode was set to acquire one high resolution MS scan in the ICR cell followed by three collision induced

dissociation MS/MS scans in the linear ion trap. For a high resolution MS scan, 10^6 ions were accumulated over a maximum time of 500 ms and the FWHM resolution was set to 60,000 (at m/z 300). Only MS signals exceeding 500 ion counts triggered a MS/MS attempt and 10^4 ions were acquired for a MS/MS scan over a maximum time of 250 ms. The normalized collision energy was set to 35% and one microscan was acquired for each spectrum. Singly charged ions were excluded from triggering MS/MS scans.

All acquired MS/MS spectra were searched against the International Protein Index (IPI) database (Version 3.26) using the Sequest algorithm. The Sequest database search criteria included: 0.2 Da mass tolerance for the precursor ion, 0.5 Da mass tolerance for the fragment ions, variable modifications of 0.984016 Da for asparagines (representing formerly N-glycosylated asparagines after deamidation through the PNGaseF treatment) and 15.994915 Da for methionines (covering rapidly oxidizing methionines), carbamidomethylation as static modification for cysteines, at least one tryptic terminus, two missed cleavage sites. Statistical analysis of the data, including peptide and protein identification was performed using the Trans-Proteomic Pipeline v4.3 (TPP) including PeptideProphet and ProteinProphet [45-47]. Peptides and proteins were detected and quantified at a confidence score of >1.3 using the TPP in combination with Progenesis software. The ProteinProphet probability score was set such that the false discovery rate was less than 1% determined by ProteinProphet.

All MS data from this study can be downloaded in the open source mzXML format from (http://www.peptideatlas.org/repository/) and was integrated into the publicly accessible PeptideAtlas database at (http://www.peptideatlas.org/).

Labelfree Quantification

Protein quantification was performed using Progenesis (Nonlinear Dynamics). After manually improving the alignment, quantified peaks were filtered for identification by sequence search and overall protein abundances were calculated thereof. Significance of detected differences were assessed with ANOVAs.

Animal Husbandry

All of the mice used in this study were CD1 mice obtained from the Jackson laboratories and housed in accordance with the Institutional and Governmental Animal Care Committee guidelines of the University of Toronto.

Morula Aggregations

8-cell ES, pNSC or dNSC colonies were aggregated with diploid CD1 morula for 24 hr as described in [48], and embryos were then transplanted into pseudo-pregnant CD1 females.

N-Cadherin Aggregation Assay. pNSCs were passaged into SFM +FGF2 +B27 as described previously, with the addition of 0.8ug/ml N-Cad function-blocking antibody (Sigma) during plating. 0.8ug/ml was also added to KSOM during the overnight aggregation.

Imaging

Sections of chimeras were imaged using a 40x/0.60 Olympus IX81 inverted microscope with the Olympus Microsuite Version 3.2 Analysis imaging system software (Soft Imaging System). Overnight integration into the ICM was visualized with the same setup, and confirmed in a subset of cases with confocal imaging. Sections of embryoid bodies were taken with ZeissAxio Observer.D1 inverted fluorescent microscope equipped with an AxioCamMrm digital camera run by AxioVision v4.8 software.

Confocal. Images of morula aggregations involving the N-cad function-blocking antibody were taken with an Olympus IX81 inverted microscope with the Olympus FV10-ASW v2.01. Images of dsRed chimeric embryos were taken every 5 μm with a Leica TCS2 confocal microscope.

Immunocytochemistry

Sections were permeabilized with 0.3% Triton X-100 detergent (Sigma), sequentially blocked with 1% bovine serum albumin (Sigma), followed by 10% normal goat serum (NGS)(Sigma) in Stockholm's PBS + 0.3% Triton X, pH 7.3 for 30 min at room temperature before application of primary antibodies overnight in Stockholm's PBS, 1.0% NGS, and 0.3% Triton X-100. Primary anti-smooth muscle actin was applied at 1:250 (Sigma). Sections were washed and re-blocked as above before applying the secondary antibodies at 37°C for 2 hr in Stockholm's PBS + 1.0% NGS. Goat anti-mouse 568 nm Alexa Fluor antibodies (1:333; Invitrogen) was used as a secondary. Nuclei were counterstained with 10 µg/ml Hoechst 33258 (Sigma) before samples were mounted and coverslips applied using Gel Mount (Biomeda).

Quantitative PCR

QPCR was performed using Taqman Assays (Applied Biosystems; AB) according to the manufacturer's instructions on a 7900 HT Fast-Time PCR System (AB) and analyzed with SDS v2.3 software. The following Taqman Assays were used: EphA4 (Mm00433056_m1; AB), Rplp0 (Mm99999223_gH; AB) and cKit (Mm00445212_m1; AB). We tried to measure Erbb2 abundance using two Taqman Assays (Mm00658541_m1 and Mm01306783_m1; AB), but did not obtain reliable results due to low transcript abundance.

ACKNOWLEDGMENTS

Thanks to Laurie Sellings and Lilian Doss for help with the statistics, Marina Gertsenstein for technical expertise as well as Andras Nagy for reagents. The work was funded by CIHR (to D.v.d.K.) and from the NCCR Neural Plasticity and Repair (to B.W.). The authors report no competing interests.

REFERENCES

1. Gaulden, J., and Reiter, J.F. (2008). Neur-ons and neur-offs: regulators of neural induction in vertebrate embryos and embryonic stem cells. Hum Mol Genet *17*, R60-66.
2. Ying, Q.L., Nichols, J., Chambers, I., and Smith, A. (2003). BMP induction of Id proteins suppresses differentiation and sustains embryonic stem cell self-renewal in collaboration with STAT3. Cell *115*, 281-292.
3. Tropepe, V., Hitoshi, S., Sirard, C., Mak, T.W., Rossant, J., and van der Kooy, D. (2001). Direct neural fate specification from embryonic stem cells: a primitive mammalian neural stem cell stage acquired through a default mechanism. Neuron *30*, 65-78.
4. Chambers, I., and Smith, A. (2004). Self-renewal of teratocarcinoma and embryonic stem cells. Oncogene *23*, 7150-7160.
5. Smukler, S.R., Runciman, S.B., Xu, S., and van der Kooy, D. (2006). Embryonic stem cells assume a primitive neural stem cell fate in the absence of extrinsic influences. J Cell Biol *172*, 79-90.
6. Yates, A., and Chambers, I. (2005). The homeodomain protein Nanog and pluripotency in mouse embryonic stem cells. Biochem Soc Trans *33*, 1518-1521.
7. Hollnagel, A., Oehlmann, V., Heymer, J., Ruther, U., and Nordheim, A. (1999). Id genes are direct targets of bone morphogenetic protein induction in embryonic stem cells. J Biol Chem *274*, 19838-19845.
8. Hitoshi, S., Seaberg, R.M., Koscik, C., Alexson, T., Kusunoki, S., Kanazawa, I., Tsuji, S., and van der Kooy, D. (2004). Primitive neural stem cells from the mammalian epiblast differentiate to definitive neural stem cells under the control of Notch signaling. Genes Dev *18*, 1806-1811.
9. Mathis, L., Kulesa, P.M., and Fraser, S.E. (2001). FGF receptor signalling is required to maintain neural progenitors during Hensen's node progression. Nat Cell Biol *3*, 559-566.
10. Kunath, T., Saba-El-Leil, M.K., Almousailleakh, M., Wray, J., Meloche, S., and Smith, A. (2007). FGF stimulation of the Erk1/2 signalling cascade triggers transition of pluripotent embryonic stem cells from self-renewal to lineage commitment. Development *134*, 2895-2902.
11. Wollscheid, B., Bausch-Fluck, D., Henderson, C., O'Brien, R., Bibel, M., Schiess, R., Aebersold, R., and Watts, J.D. (2009). Mass-spectrometric identification and relative quantification of N-linked cell surface glycoproteins. Nat Biotechnol *27*, 378-386.
12. Lu, R., Markowetz, F., Unwin, R.D., Leek, J.T., Airoldi, E.M., MacArthur, B.D., Lachmann, A., Rozov,

R., Ma'ayan, A., Boyer, L.A., et al. (2009). Systems-level dynamic analyses of fate change in murine embryonic stem cells. Nature *462*, 358-362.
13. Hofmann, A., Gerrits, B., Schmidt, A., Bock, T., Bausch-Fluck, D., Aebersold, R., and Wollscheid, B. Proteomic cell surface phenotyping of differentiating acute myeloid leukemia cells. Blood *116*, e26-34.
14. Schiess, R., Mueller, L.N., Schmidt, A., Mueller, M., Wollscheid, B., and Aebersold, R. (2009). Analysis of cell surface proteome changes via label-free, quantitative mass spectrometry. Mol Cell Proteomics *8*, 624-638.
15. Apweiler, R., Hermjakob, H., and Sharon, N. (1999). On the frequency of protein glycosylation, as deduced from analysis of the SWISS-PROT database. Biochim Biophys Acta *1473*, 4-8.
16. Zielinska, D.F., Gnad, F., Wisniewski, J.R., and Mann, M. Precision mapping of an in vivo N-glycoproteome reveals rigid topological and sequence constraints. Cell *141*, 897-907.
17. Shannon, P., Markiel, A., Ozier, O., Baliga, N.S., Wang, J.T., Ramage, D., Amin, N., Schwikowski, B., and Ideker, T. (2003). Cytoscape: a software environment for integrated models of biomolecular interaction networks. Genome Res *13*, 2498-2504.
18. Uchida, N., Buck, D.W., He, D., Reitsma, M.J., Masek, M., Phan, T.V., Tsukamoto, A.S., Gage, F.H., and Weissman, I.L. (2000). Direct isolation of human central nervous system stem cells. Proc Natl Acad Sci U S A *97*, 14720-14725.
19. Furne, C., Ricard, J., Cabrera, J.R., Pays, L., Bethea, J.R., Mehlen, P., and Liebl, D.J. (2009). EphrinB3 is an anti-apoptotic ligand that inhibits the dependence receptor functions of EphA4 receptors during adult neurogenesis. Biochim Biophys Acta *1793*, 231-238.
20. Ricard, J., Salinas, J., Garcia, L., and Liebl, D.J. (2006). EphrinB3 regulates cell proliferation and survival in adult neurogenesis. Mol Cell Neurosci *31*, 713-722.
21. Pruszak, J., Ludwig, W., Blak, A., Alavian, K., and Isacson, O. (2009). CD15, CD24, and CD29 define a surface biomarker code for neural lineage differentiation of stem cells. Stem Cells *27*, 2928-2940.
22. Pastrana, E., Cheng, L.C., and Doetsch, F. (2009). Simultaneous prospective purification of adult subventricular zone neural stem cells and their progeny. Proc Natl Acad Sci U S A *106*, 6387-6392.
23. Picotti, P., Bodenmiller, B., Mueller, L.N., Domon, B., and Aebersold, R. (2009). Full dynamic range proteome analysis of S. cerevisiae by targeted proteomics. Cell *138*, 795-806.
24. Riethmacher, D., Brinkmann, V., and Birchmeier, C. (1995). A targeted mutation in the mouse E-cadherin gene results in defective preimplantation development. Proc Natl Acad Sci U S A *92*, 855-859.
25. Karpowicz, P., Inoue, T., Runciman, S., Deveale, B., Seaberg, R., Gertsenstein, M., Byers, L., Yamanaka, Y., Tondat, S., Slevin, J., et al. (2007). Adhesion is prerequisite, but alone insufficient, to elicit stem cell pluripotency. J Neurosci *27*, 5437-5447.
26. Zhang, P., Gao, W.Y., Turner, S., and Ducatman, B.S. (2003). Gleevec (STI-571) inhibits lung cancer cell growth (A549) and potentiates the cisplatin effect in vitro. Mol Cancer *2*, 1.
27. Taipale, J., Chen, J.K., Cooper, M.K., Wang, B., Mann, R.K., Milenkovic, L., Scott, M.P., and Beachy, P.A. (2000). Effects of oncogenic mutations in Smoothened and Patched can be reversed by cyclopamine. Nature *406*, 1005-1009.
28. Fabes, J., Anderson, P., Brennan, C., and Bolsover, S. (2007). Regeneration-enhancing effects of EphA4 blocking peptide following corticospinal tract injury in adult rat spinal cord. Eur J Neurosci *26*, 2496-2505.
29. Kanakry, C.G., Li, Z., Nakai, Y., Sei, Y., and Weinberger, D.R. (2007). Neuregulin-1 regulates cell adhesion via an ErbB2/phosphoinositide-3 kinase/Akt-dependent pathway: potential implications for schizophrenia and cancer. PLoS One *2*, e1369.
30. Karpowicz, P., Willaime-Morawek, S., Balenci, L., DeVeale, B., Inoue, T., and van der Kooy, D. (2009). E-Cadherin regulates neural stem cell self-renewal. J Neurosci *29*, 3885-3896.
31. Machold, R., Hayashi, S., Rutlin, M., Muzumdar, M.D., Nery, S., Corbin, J.G., Gritli-Linde, A., Dellovade, T., Porter, J.A., Rubin, L.L., et al. (2003). Sonic hedgehog is required for progenitor cell maintenance in telencephalic stem cell niches. Neuron *39*, 937-950.
32. Ying, Q.L., Wray, J., Nichols, J., Batlle-Morera, L., Doble, B., Woodgett, J., Cohen, P., and Smith, A. (2008). The ground state of embryonic stem cell self-renewal. Nature *453*, 519-523.
33. Balordi, F., and Fishell, G. (2007). Mosaic removal of hedgehog signaling in the adult SVZ reveals that the residual wild-type stem cells have a limited capacity for self-renewal. J Neurosci *27*, 14248-14259.
34. Brons, I.G., Smithers, L.E., Trotter, M.W., Rugg-Gunn, P., Sun, B., Chuva de Sousa Lopes, S.M., Howlett, S.K., Clarkson, A., Ahrlund-Richter, L., Pedersen, R.A., et al. (2007). Derivation of pluripotent epiblast stem cells from mammalian embryos. Nature *448*, 191-195.
35. Tesar, P.J., Chenoweth, J.G., Brook, F.A., Davies, T.J., Evans, E.P., Mack, D.L., Gardner, R.L., and McKay, R.D. (2007). New cell lines from mouse epiblast share defining features with human embryonic stem cells. Nature *448*, 196-199.
36. Bao, S., Tang, F., Li, X., Hayashi, K., Gillich, A., Lao, K., and Surani, M.A. (2009). Epigenetic reversion of post-implantation epiblast to pluripotent embryonic stem cells. Nature *461*, 1292-1295.
37. Calaora, V., Rogister, B., Bismuth, K., Murray, K., Brandt, H., Leprince, P., Marchionni, M., and Dubois-Dalcq, M. (2001). Neuregulin signaling regulates neural precursor growth and the generation of oligodendrocytes in vitro. J Neurosci *21*, 4740-4751.

38. Hadjantonakis, A.K., Macmaster, S., and Nagy, A. (2002). Embryonic stem cells and mice expressing different GFP variants for multiple non-invasive reporter usage within a single animal. BMC Biotechnol *2*, 11.
39. Rossant, N.a. (1993). Production of a complete ES cell derived fetus, (Oxford, UK: IRL Press).
40. Cooper, M.K., Porter, J.A., Young, K.E., and Beachy, P.A. (1998). Teratogen-mediated inhibition of target tissue response to Shh signaling. Science *280*, 1603-1607.
41. Murai, K.K., Nguyen, L.N., Koolpe, M., McLennan, R., Krull, C.E., and Pasquale, E.B. (2003). Targeting the EphA4 receptor in the nervous system with biologically active peptides. Mol Cell Neurosci *24*, 1000-1011.
42. Baker, B.E., Kestler, D.P., and Ichiki, A.T. (2006). Effects of siRNAs in combination with Gleevec on K-562 cell proliferation and Bcr-Abl expression. J Biomed Sci *13*, 499-507.
43. Manley, P.W., Cowan-Jacob, S.W., Buchdunger, E., Fabbro, D., Fendrich, G., Furet, P., Meyer, T., and Zimmermann, J. (2002). Imatinib: a selective tyrosine kinase inhibitor. Eur J Cancer *38 Suppl 5*, S19-27.
44. Eisele, Y.S., Baumann, M., Klebl, B., Nordhammer, C., Jucker, M., and Kilger, E. (2007). Gleevec increases levels of the amyloid precursor protein intracellular domain and of the amyloid-beta degrading enzyme neprilysin. Mol Biol Cell *18*, 3591-3600.
45. Keller, A., Nesvizhskii, A.I., Kolker, E., and Aebersold, R. (2002). Empirical statistical model to estimate the accuracy of peptide identifications made by MS/MS and database search. Anal Chem *74*, 5383-5392.
46. Nesvizhskii, A.I., Keller, A., Kolker, E., and Aebersold, R. (2003). A statistical model for identifying proteins by tandem mass spectrometry. Anal Chem *75*, 4646-4658.
47. Deutsch, E.W., Mendoza, L., Shteynberg, D., Farrah, T., Lam, H., Tasman, N., Sun, Z., Nilsson, E., Pratt, B., Prazen, B., et al. A guided tour of the Trans-Proteomic Pipeline. Proteomics *10*, 1150-1159.
48. Wood, S.A., Allen, N.D., Rossant, J., Auerbach, A., and Nagy, A. (1993). Non-injection methods for the production of embryonic stem cell-embryo chimaeras. Nature *365*, 87-89.

See www.StemCells.com for supporting information available online.

Figure 1. Overview of CSC-based protein identifications. A Summary of the experimental replicates, as well as aggregate peptide and protein identifications in each cell type. B Schematic depicting the number of unique membrane proteins, predicted by Transmembrane Hidden Markov Model, identified in each cell type by ProteinProphet and the overlap between them. C The schematic depicts proteins (grey balls) which differ significantly in abundance between at least two cell types in the lineage ($p<0.05$), and are 5 times more abundant in the cell type (blue balls) to which they are connected with an edge than those to which they are not connected.

Fig 1.

A

Overview of shotgun identifications

Cell Type	Biological replicates	Technical replicates	Identified proteins, FDR <0.01	Identified peptides	NXST specificity (%)
ES	2	4	378	813	84
pNCS	3	7	563	1134	71
dNCS	2	4	456	880	90
Total	7	15	743	1748	76

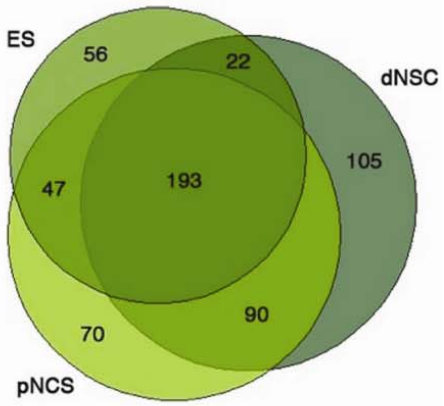

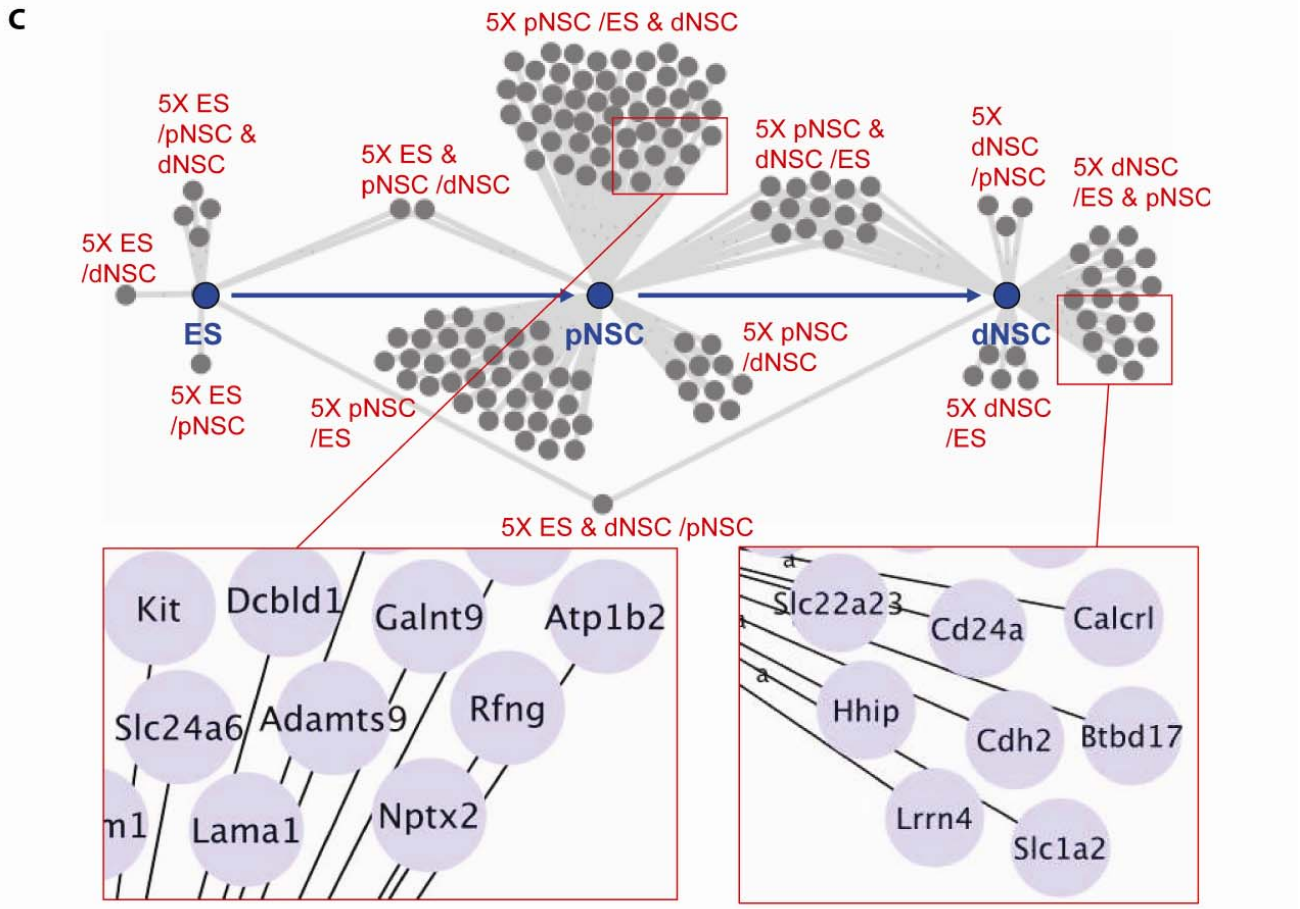

Figure 2. NSCs lose the ability to colonize the ICM as they mature through the lineage. A Contribution of YFP+ ES cells (green) to the ICM (*) is apparent in 2 of 3 blastocysts in this representative image. The scale bar is 50μm. B Quantification of the frequency with which donor cells colonize the embryo at the developmental timepoints indicated. Contribution at E3.5 was scored positive if integration within the ICM occurred after overnight integration, and at E9.5 if embryos were partially fluorescent. Note that embryos were sorted at E3.5 such that only embryos with donor contribution to the ICM were reimplanted into surrogate mothers. The latter timepoint reflects this. pNSCs persisted to E9.5 in 48 of 52 cases compared to 9 of 19 blastocysts colonized by NSC +Lif +Fgf, and 1 of 5 in the case of dNSCs. C The relative abundance of E-cad was measured using quantitative PCR (± s.e.m.). The data is normalized to abundance in ES cells.

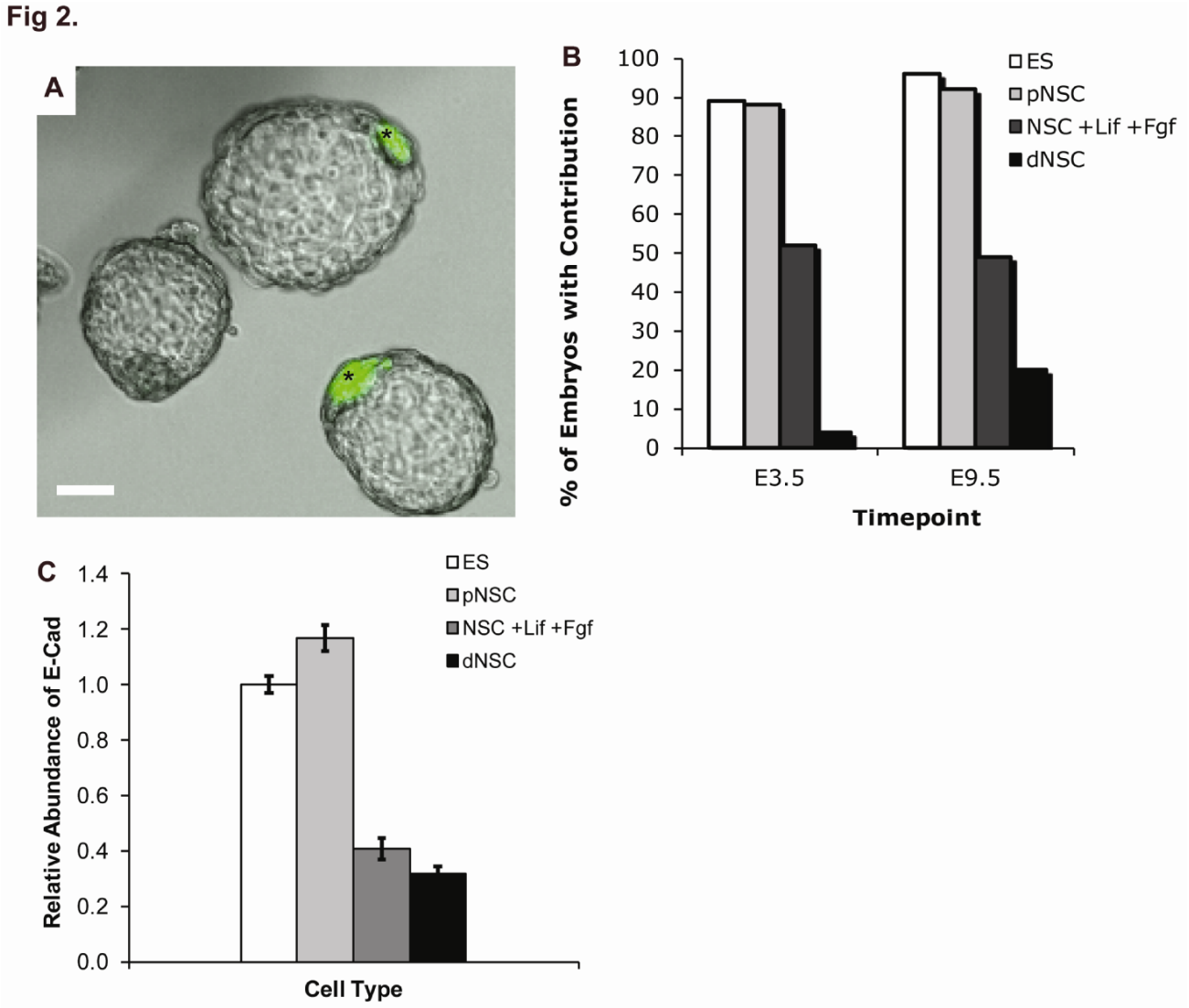

Figure 3. Up-regulation of N-cad prevents dNSCs from aggregating with morula A 3-dimensional peaks used to quantify the abundance of N-cad. The relative MS integrated peak area signal of the N-cad peptide in the ES cell sample (left) is compared to the equivalent peak area signal in the dNSC sample (right). The peak area within the red box was selected, fragmented and resulting spectra identified as N-cad peptides by SEQUEST based database searching. B Culturing dNSCs in N-cad function-blocking antibody partially rescues the ability of dNSCs to colonize the ICM. Integration frequency within the ICM was quantified and is depicted ± s.t.d. (aggregate counts are: ES n= 45, dNSC n= 25, dNSC + N-cad antibody n= 83). C Sample image of dNSC aggregation (scale bar =50μm). DI-IV Representative optical sections (spaced by 10μm in a single confocal Z-stack) confirming that blocking N-cad in dNSCs rescues ICM colonization.

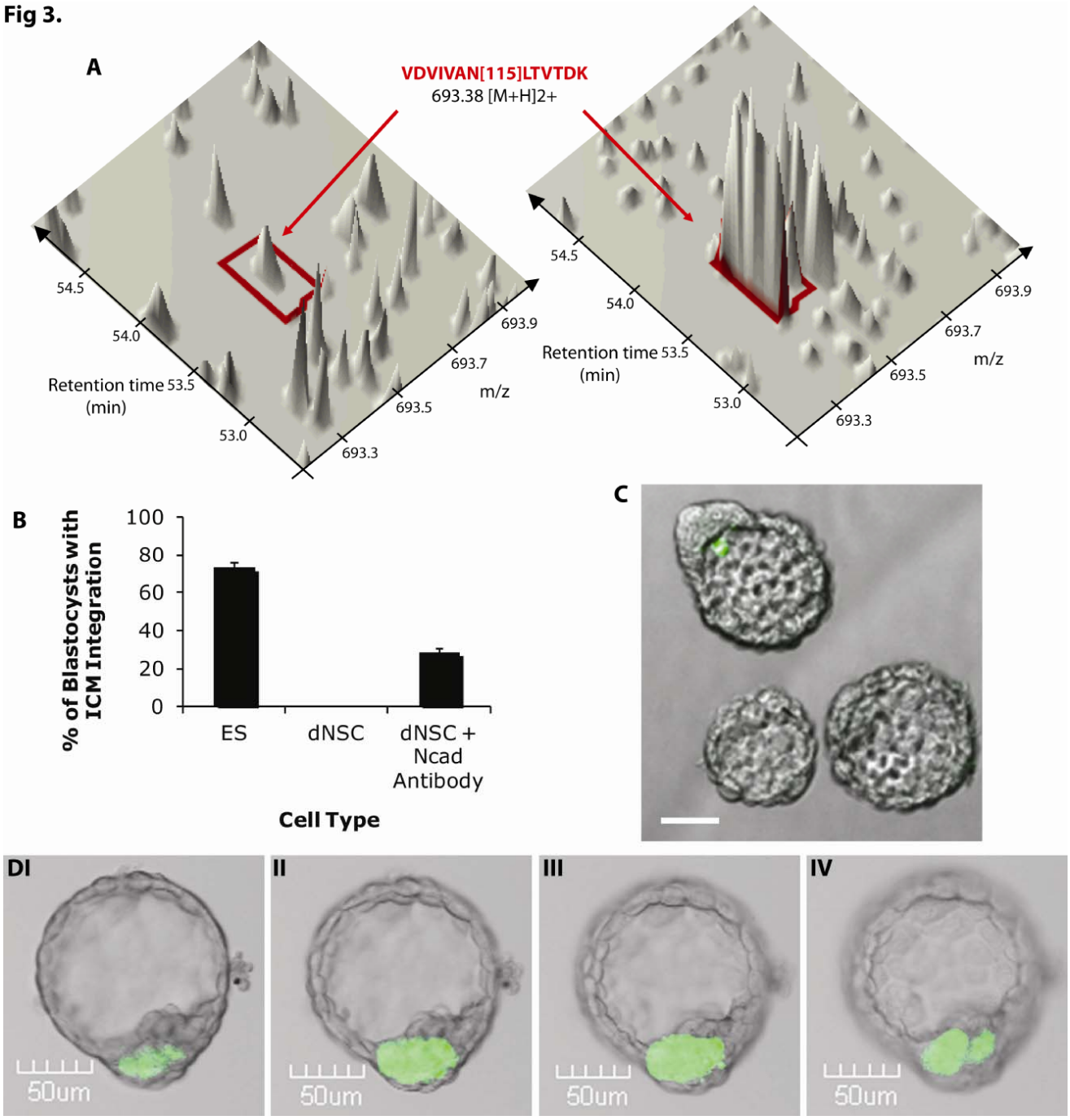

Figure 4. The ES-derived neural lineage predicts molecules that are functionally relevant for NSCs derived from adult mice. A Proteins found to be highly enriched in either pNSCs or dNSCs relative to ES cells were inhibited with Erbb2 inhibitor II, Cyclopamine (Hedgehog signaling; Hh), Gleevec (c-kit) or an EphA4 blocking peptide. ES cells were grown in serum and Lif, pNSCs in serum free media and Lif, and dNSCs in serum free media and FGF + B27 for this comparison. The frequency of 50μm colony formation was then compared between the different populations after normalizing to an appropriate vehicle control for each inhibitor. The normalized frequency of colony formation is depicted ± s.e.m. An ANOVA was used to assess significance ($F_{3,15} = 8.27$, $p<0.05$). The Erbb2 inhibitor blocked pNSC formation without impairing either ES or dNSC colony-formation, *$p<0.05$. Cyclopamine blocked the formation of both pNSCs and dNSCs (*$p<0.05$), as did the EphA4 inhibitor peptide *$p<0.05$. Conversely, Gleevec enhanced pNSC formation *$p<0.05$, but did not affect colony formation of either ES or dNSCs. Notably, inhibitors which blocked the formation of ES-derived NSCs, also blocked the formation of adult mouse derived NSCs. The Erbb2 inhibitor, Cyclopamine and the EphA4 inhibitor peptide all blocked aNSC formation *$p<0.05$. In the case of Gleevec, it impaired aNSC formation, in contrast to its lack of effect on ES-derived dNSCs and promotion of pNSC formation. B EphA4 and Hh have significant effects on NSC survival, *$p<0.05$. Viability after 24hrs and is depicted ± s.e.m. Viability in Erbb2 inhibitor and Gleevec was unaffected. C pNSC colony size (depicted ± s.e.m) was quantified in the presence of 4uM Gleevec and no difference was apparent relative to the vehicle control, indicating that the increase of pNSC colony formation in the presence of Gleevec is not the result of increased proliferation.

Fig 4.

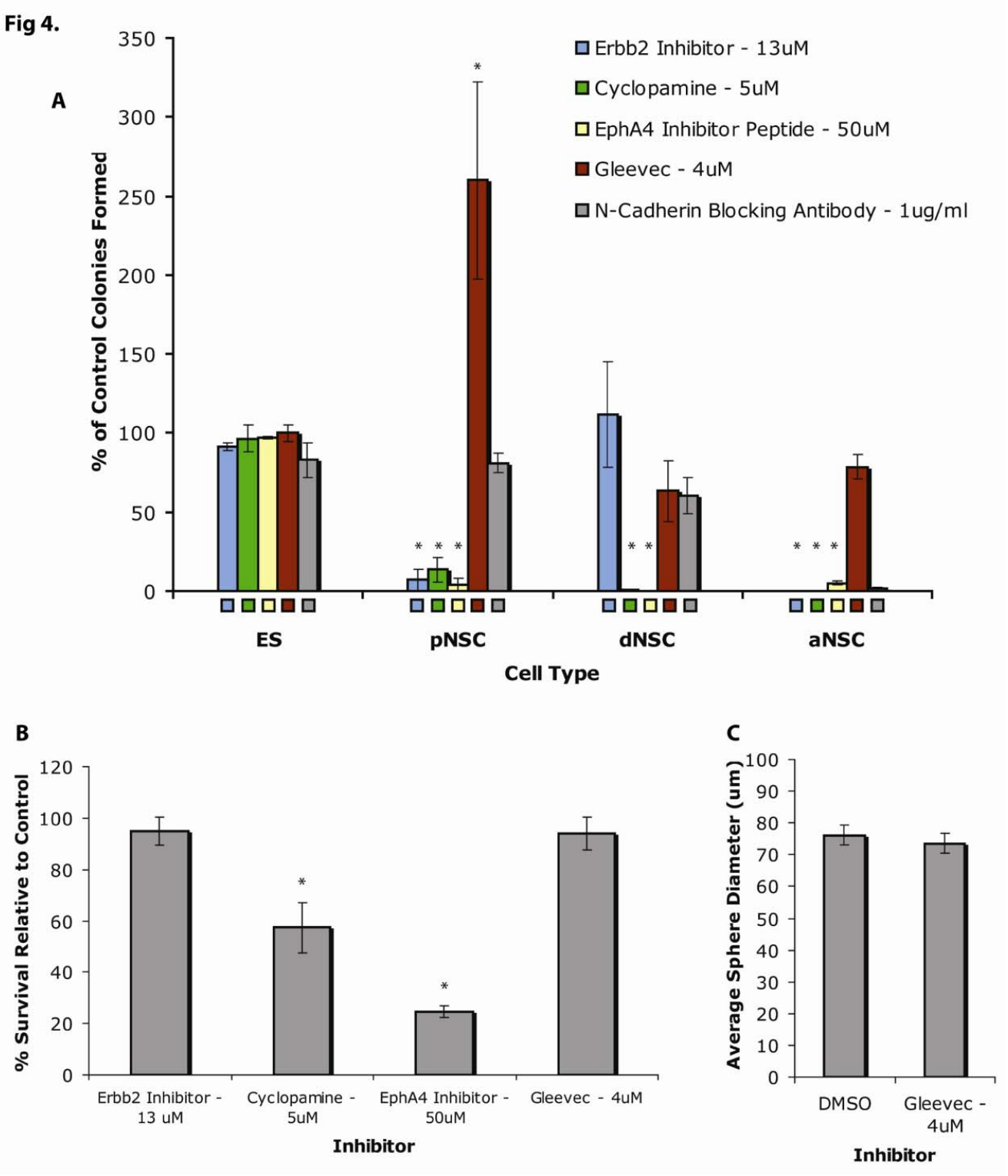
A
% of Control Colonies Formed
350
300
250
200
150
100
50
0
Erbb2 Inhibitor - 13uM
Cyclopamine - 5uM
EphA4 Inhibitor Peptide - 50uM
Gleevec - 4uM
N-Cadherin Blocking Antibody - 1ug/ml
ES
pNSC
dNSC
aNSC
Cell Type
B
% Survival Relative to Control
120
100
80
60
40
20
0
Erbb2 Inhibitor - 13 uM
Cyclopamine - 5uM
EphA4 Inhibitor - 50uM
Gleevec - 4uM
Inhibitor
C
Average Sphere Diameter (um)
100
90
80
70
60
50
40
30
20
10
0
DMSO
Gleevec - 4uM
Inhibitor

Figure 5. siRNA validates identity of candidates implicated in NSC function. A,B Quantitative PCR supports depletion of intended transcripts ($p<0.05$, two-tailed student t-tests). Relative abundance of EphA4 (A) and c-kit (B) transcripts in pNSC cultures following treatment with siRNAs targeting these respective transcripts (depicted ± s.e.m). C siRNA confirmed the effects of targeting candidates with inhibitors. The candidates implicated in NSC function with inhibitors (Fig 4) were targeted with siRNAs and assayed equivalently to confirm that the putative candidates were responsible for the observed effects. Treatments were normalized to a Scramble control as opposed to vehicle and depicted as the frequency of colony formation ± s.e.m. siRNA targeting Erbb2 and EphA4 decreased pNSC formation, while c-kit depletion increased it ($F_{3,11} = 28.03$, $p<0.05$). These effects and those of siRNA on dNSCs replicate the positive effects that small molecules had on NSCs (compare with Fig 4A).

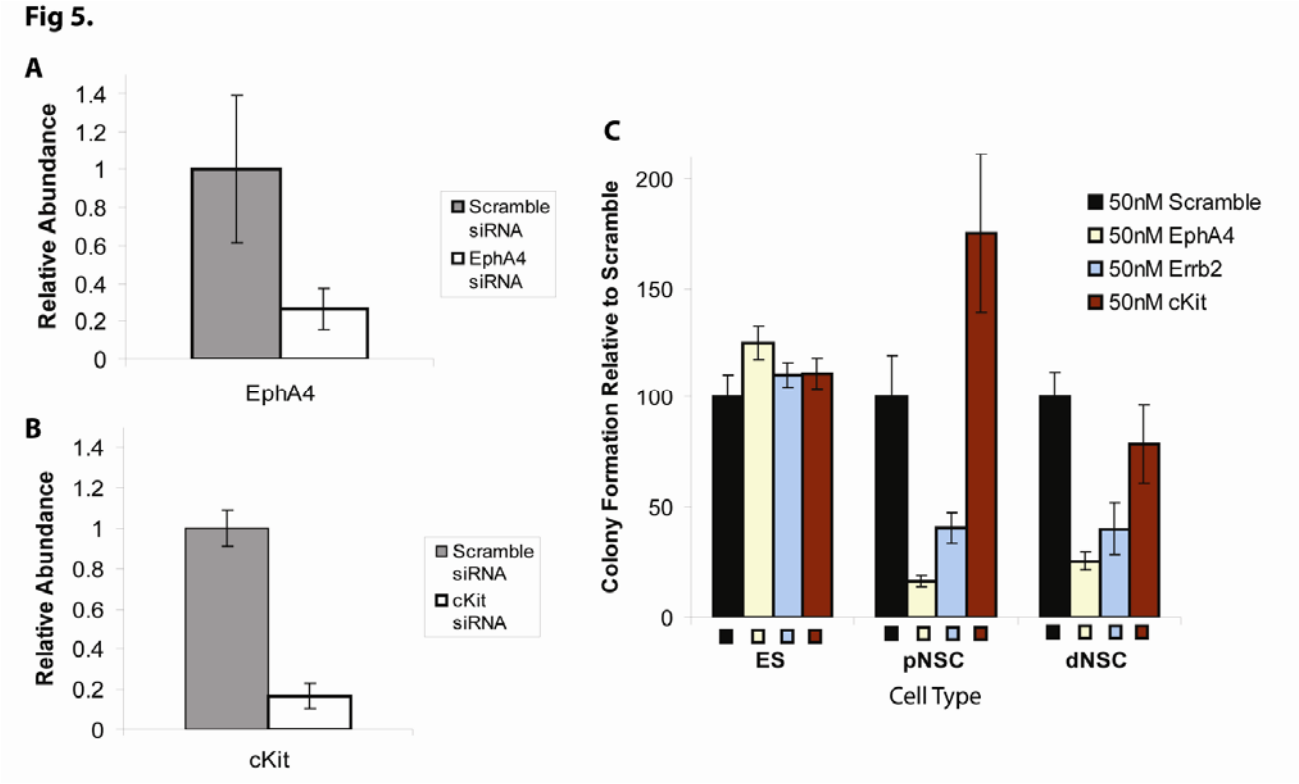

Figure 6. Schematic summarizing the neural maturation model, with novel regulators implicated by this project in blue text.